Soft Matter

PAPER

View Article Online
View Journal | View Issue

Cite this: *Soft Matter*, 2024, **20**, 2584

Simultaneous coupling of metal removal and visual detection by nature-inspired polyphenol-amine surface chemistry†

Helen H. Ju, Hong K. Park, Jingxian Wu, Yu Ri Nam, Eunu Kim, Jeongin Seo and Haeshin Lee *

Received 11th October 2023,
Accepted 26th January 2024

DOI: 10.1039/d3sm01363d

rsc.li/soft-matter-journal

The interplay between polyphenols, amines, and metals has broad implications for surface chemistry, biomaterials, energy storage, and environmental science. Traditionally, polyphenol–amine combinations have been recognized for their ability to form adhesive, material-independent thin layers that offer a diverse range of surface functionalities. Herein, we demonstrate that a coating of tannic acid (TA) and polyethyleneimine (PEI) provides an efficient platform for capturing and monitoring metal ions in water. A unique feature of our PEI/TA-coated microbeads is the '**Detec**tion-Cap**ture**' (**Detec-Ture**) mechanism. The galloyl groups in TA coordinate with Fe(III) ions (capture), initiating their oxidation to gallol–quinone. These oxidized groups subsequently react with PEI amines, leading to the formation of an Fe(II/III)–gallol–PEI network that produces a vivid purple color, thereby enabling visual detection. This mechanism couples metal capture directly with detection, distinguishing our approach from existing studies, which have either solely focused on metal removal or metal detection. The metal capturing capacity of our materials stands at 0.55 mg g^{-1}, comparable to that of established materials like alginate and wollastonite. The detection sensitivity reaches down to 0.5 ppm. Our findings introduce a novel approach to the utility of metal–polyphenol–amine networks, presenting a new class of materials suited for simultaneous metal ion detection and capture in environmental applications.

Introduction

The development of polyphenolic chemistry has significantly advanced the field of surface science. Initiated by the pioneering study on substrate-independent surface chemistry facilitated by polydopamine coatings,[1] a plethora of subsequent studies have emerged, exploring diverse polyphenolic moieties to broaden the scope of surface functionalities. Among these, Sileika *et al.* have developed multifunctional surface chemistry, utilizing trihydroxybenzene (*i.e.*, galloyl) functional groups, such as pyrogallol (PG) and tannic acid (TA).[2] This material-independent coating has been applied to a wide array of organic and inorganic substrates, including poly(carbonate), poly(tetrafluoroethylene), stainless steel, metal nanoparticles, and others, demonstrating antibacterial and antioxidant properties.

The interplay between amines and polyphenols plays a pivotal role in insect biochemistry.[3] For instance, the initial sclerotization of a fragile cuticle layer leads to a mechanically robust structure *via* oxidative catecholamine cross-linking as it ages.[4] Studies have elucidated how amine-rich histidyl residues in cuticular proteins form cross-links with catechol-derived phenolic quinones, serving as the backbone of insect exoskeletal cuticles.[5,6] Inspired by this natural phenomenon, scientists have engineered biomimetic polyphenol–amine chemistry at interfaces. Hong *et al.* demonstrated the chemical synergy between amine and galloyl groups using a model small molecule, 5-pyrogallol 2-aminoethane (PAE).[7] The incorporation of primary amine substantially enhanced the coating stability across various materials compared to coatings with amine-absent galloyl molecules, like tannic acid. Moreover, Hong *et al.* extended their work beyond examining the inter-molecular attributes of amine-containing polymers and phenolic molecules. By using catechol/catecholamine small molecules and poly(ethyleneimine) (PEI), they illustrated an intermolecular, bio-mimetic oxidative interfacial cross-linking reaction that mimics an insect's protective exoskeleton.[8] Their findings suggest that catechol/catecholamine cross-linking is particularly effective at air–water interfaces where oxygen is rich, explaining the increased mechanical rigidity of external cuticle layers compared to inner layers. Sequentially, Park *et al.* developed a protective coating using gallolamine

Department of Chemistry, KAIST (Korea Advanced Institute of Science and Technology), Daehak-ro, Yuseong-gu, Daejeon 34141, Republic of Korea. E-mail: haeshin@kaist.ac.kr

† Electronic supplementary information (ESI) available. See DOI: https://doi.org/10.1039/d3sm01363d

chemistry at the air–water interface.[9] This synthetic, exoskeleton-like coating exhibited resilient properties under harsh external conditions such as dehydration, shrinkage, and temperature variations.

Although the synergy between polyphenols and amines offers remarkable stability at the interface, the interaction of polyphenols with metal ions offers an additional avenue of exploration. A notable example of this area was introduced by Ejima *et al.* through the development of metal–phenolic networks (MPNs).[10] They reported the chelation chemistry between phenolic galloyl ligands, such as tannic acid, and inorganic cross-linkers like ferric ions, leading to the formation of various structured metal–galloyl frameworks. However, a limitation of MPNs is their reliance on the metal cross-linker for structure formation. Nature offers examples of similar phenol–metal interactions, evident in siderophore-mediated iron chelation systems. For instance, enterobactin is secreted by *E. coli* to secure iron,[11] while another siderophore, cyclic trichrysobactin, is produced by the plant *Dickeya chrysanthemi* to protect itself against pathogens.[12] Both siderophores employ multiple phenolic (catechol) moieties for robust interaction with metal ions.

While the fields of polyphenol–amine and polyphenol–metal surface chemistries have evolved largely in parallel, integrated studies embracing all three components–polyphenols, amines, and metals–are scarce. This gap in the literature presents an opportunity for potential studies to harness the synergistic potentials of these interactions. Building on this insight, we propose that a robust, conformal coating derived from polyphenol–amine (specifically, TA–PEI) interactions could serve as an effective platform for sequestration of iron ions in water with real-time monitoring capabilities. We introduce a unique surface chemistry, termed 'Detec-Ture', for simultaneous detection and capture. This dual-function mechanism sets our approach apart from existing studies, which traditionally emphasize either metal removal or detection. Upon iron–ion binding, a redox coupling facilitates iron reduction (III to II) and galloyl's oxidation to galloyl–quinone, further prompting amine–galloyl covalent reactions. The resulting metal–galloyl–amine networks manifest distinctive coating, enabling concurrent metal removal and visual detection. Iron, although non-toxic, presents its unique set of challenges due to its abundance and difficulty in removal. Its widespread presence in drinking water systems necessitates effective methods to control its concentration in water. Our gallolamine-functionalized surface introduces a groundbreaking technique to regulate and monitor waterborne iron concentration, suggesting potential applications in addressing diseases stemming from iron overload/accumulation,[13] such as secondary hemochromatosis. Notably, our methodology addresses iron concentration without relying on energy-intensive reverse osmosis or intricate pH control methods.[14,15] In a testament to its efficacy, PEI/TA-coated beads were able to visually detect iron from a 10 ppm Fe(III) solution in just 20 seconds, boasting a sensitivity threshold down to 1 ppm. Furthermore, one gram of PEI/TA-coated beads adsorbed 0.55 mg of iron ions, showcasing the rapid and robust adsorption capabilities of our formulation.

Experimental

Materials

Poly(ethyleneimine) (branched, M.W. = 750 000), tannic acid (M.W. = 1701.20), and iron(III) chloride (M.W. = 162.20) were ordered from Sigma Aldrich, South Korea. Sephadex G-75 (particle size = 90–280 μm (wet)) was ordered from GE Healthcare, Sweden. An Econo-Pac® chromatography column (pore size = 30 μm) was ordered from Bio-Rad, South Korea. Teabag was purchased from a dollar store, South Korea.

PEI/TA coating procedures

PEI and TA were separately dissolved in double-distilled water (DDW). The final concentration of both PEI and TA was 0.01 wt%. Dextran bead powder (10 mg) was swollen and washed with 500 mL of DDW ahead of coating. Excessive DDW was drained. Subsequently, PEI solution (500 mL) was poured to the swollen bead, and the bead/PEI solution was gently shaken for 5 minutes. The excessive PEI solution was drained, and DDW (500 mL) was poured for washing. After 30 seconds of gentle shaking, DDW was drained. Subsequently, a TA solution (500 mL) was poured on the PEI-coated bead, and the PEI-coated bead/TA solution was gently shaken for 5 minutes. The excessive TA solution was drained, and DDW (500 mL) was poured for washing. After 30 seconds of gentle shaking, DDW was drained. The PEI/TA-coated beads were used in a variety of subsequent experiments.

Characterization of PEI/TA coatings

X-ray photoelectron spectroscopy (XPS). Bare, PEI-coated, and PEI/TA-coated beads were freeze-dried for 2 days, and the powders were sampled on a 0.5 × 0.5 mm^2 silicon wafer surface. The successive coatings of each PEI and TA layer were confirmed using XPS (Sigma probe, Thermo Scientific). The survey spectra were acquired over a binding energy range of 0–1350 eV, and high resolution XPS spectra were acquired over a range of 390–410 eV for N1s and 698–740 eV for Fe2p. The deconvolution of the XPS spectra was conducted with Avantage software.

Confocal microscopy. A Z-stacking function of the confocal microscope (ECLIPSE Ti2 inverted microscope; Nikon) was employed to confirm that the coating materials were 'soaked in' evenly into the bead rather than coating only the outermost surface of the bead. 300 μL of bare bead and PEI/TA-coated bead solutions were drop-cast on the confocal microscopy glass for imaging. The enhanced green fluorescent protein (EGFP) fluorescence image (emission wavelength: 525 nm; excitation wavelength: 488 nm) was merged with the differential interference contrast (DIC) image. The scale bar was inserted using Image J software.

Fe–ion adsorption experiment

Column chromatography. The swollen PEI/TA-coated beads were packed in a column until the 3 g graduation mark. 15 mL of DDW was eluted down to pack the beads remaining on the inner wall of the column. Then, 5 mL of a 10 ppm iron ion solution was eluted down the column with gravitational force. The eluted solution was collected for inductively coupled

plasma-optical emission spectrometry (ICP-OES) to measure the adsorption capacity.

Examination of Fe–ion adsorption by Raman spectroscopy. The presence of Fe–galloyl coordination bonds was confirmed with a high-resolution Raman/photoluminescence spectrophotometer (LabRAM HR Evolution Visible_NIR, HORIBA) equipped with a 785 nm excitation laser. Samples of freeze-dried PEI/TA-coated beads, both before and after Fe–ion adsorption, were prepared on glass slides for analysis. Spectra were acquired over a Raman shift range of 400–1800 cm^{-1} using a 600 mm^{-1} grating spectrograph. An integration time of 60 seconds was employed for all measurements, and each spectrum was accumulated three times with the same integration time to ensure reliability.

Fe–ion adsorption test

PEI/TA-coated beads (wet = 15.618 g; dry = 1.937 g) were immersed in a 10 ppm Fe(III) solution (300 mL) and stirred at 100 rpm. The Fe(III) concentration was measured using ICP-OES (5110 ICP-OES, Agilent) at 10-second intervals for the first 2 minutes, then every minute from 2–10 minutes, and finally every 10 minutes from 10–30 minutes.

Application of PEI/TA-coated beads

Precipitation method. PEI/TA-coated beads (wet = 100 g; dry = 3.92 g) were placed in a beaker, and 100 mL of Fe(III) solution was poured into the beaker. The mixture was stirred for 15 seconds and then the suspended beads were allowed to settle.

Tea-bag method. PEI/TA-coated beads (wet = 10 g; dry = 0.392 g) were packed into the tea-bag pouch. After sealing the pouch, the PEI/TA tea-bag was submerged into a beaker with 200 mL of 10 ppm iron(III) ion solution and a magnetic stirrer at the bottom. 5 mL of the solution was collected every 5 minutes for measuring the ion concentration with an ICP-OES instrument.

Results and discussion

The PEI/TA-coated beads were prepared by the following method. Cross-linked dextran beads, specifically Sephadex G-75, were added to a PEI solution (0.01 wt%). The volume ratio of the coating solution to the swollen bead was 5 : 3. Coatings were carried out for 5 minutes, and excess PEI was washed with distilled water. Then, identical coating and washing procedures were applied to the TA coating step (0.01 wt%).

To confirm the PEI/TA coating as depicted in Fig. 1a, we analyzed the unmodified, PEI-coated, and PEI/TA-coated beads using X-ray photoelectron spectroscopy (XPS). The presence of nitrogen-1s (N1s) photoelectrons indicated successful PEI and PEI/TA-functionalization. Given the surface sensitivity of XPS, where the probes can detect roughly up to 20 nm from the atop surface, the N1s peak from PEI might be slightly decreased due to the presence of TA that was coated over the PEI layer. As anticipated, the bare bead displayed no N1s peak (Fig. 1b, left). In contrast, the bead coated solely with PEI exhibited the N1s peaks. The N1s peak deconvolution reveals that the peak at 399.06 eV corresponds to primary amine (C–NH_2, yellow),

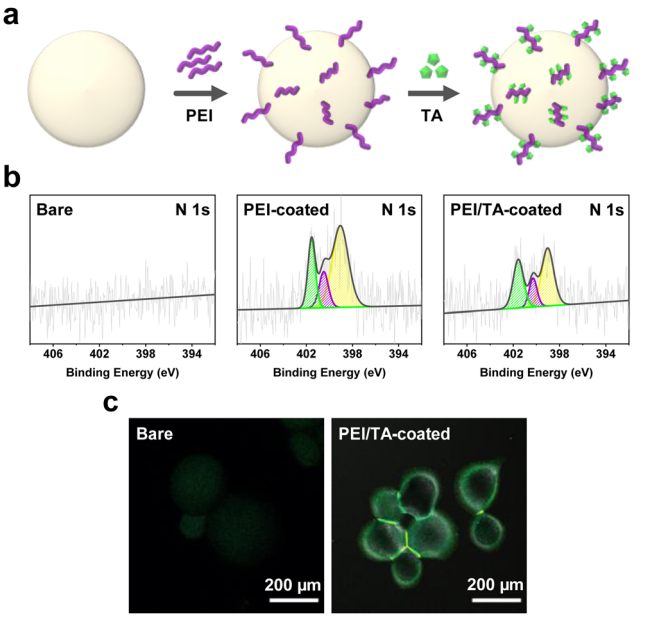

Fig. 1 Surface coating of PEI/TA on dextran beads. (a) Schematic illustration depicting the PEI/TA coating: PEI is represented by purple lines, while TA is indicated in green pentagons. (b) XPS nitrogen N1s spectra for bare (left), PEI-coated (middle), and PEI/TA-coated beads (right). (c) Confocal fluorescence microscopy images comparing bare (left) and PEI/TA-coated beads (right).

400.37 eV corresponds to secondary amine (C–NH–C, purple), and the one at 401.52 eV corresponds to tertiary amine (C–N═C, green).[16,17] The N1s spectrum of the PEI/TA-coated bead displayed peaks mirroring those from PEI. Moreover, the intensity of the N1s peak observed in the PEI/TA bead was slightly decreased compared to the one observed in the PEI-coated bead. This decrease was attributed to the surface sensitivity of the XPS technique (<20 nm), probing the ad-layer formation of tannic acid. The chemical reactivity of the galloyl group to the amine moiety results in the generation of secondary amine peaks at 400.3 eV (by Michael addition) and/or imine peaks at 401.5 eV (Schiff base formation).[16] In this case, the peak intensities corresponding to secondary amine and imine peaks should be increased relative to the peak ratio observed from PEI only (primary : secondary : tertiary = 1 : 0.32 : 0.71, Fig. 1b, middle). However, the galloyl–amine reaction occurring between TA and PEI is inconclusive, considering the slight increase in the primary: secondary: tertiary ratio (1 : 0.44 : 0.85, Fig. 1b, right) during the coating layer formation.

To validate the successful coating of PEI/TA on the beads, confocal fluorescence microscopy was employed. A previous study has elucidated that the oxidation of TA emits fluorescence signals.[18] Similar to this study, the PEI/TA-coated beads exhibit a fluorescence signal (Fig. 1c, right) due to the unavoidable oxidation of the galloyl group in the presence of dissolved oxygen as well as chemical reactions with amine groups present in PEIs. The uncoated beads showed no fluorescence signal (Fig. 1c, left).

The gallol moieties are known for their metal chelating abilities with various toxic heavy metal ions, including

Pb(II),[19–21] Mn(II),[22] and Cu(II).[23] However, their potential in addressing the removal or control of the predominant metal ion, Fe(II/III), remains relatively unexplored.[24] Instead, iron ions act either as oxidants for polyphenolic molecules, or *vice versa*, with polyphenols reducing Fe(III) to Fe(II),[25] or as coordinating metals to establish a thin metal–organic layer,[26] as illustrated in Fig. 2a. As highlighted earlier, the interplay between polyphenols and amines, specifically the tannic acid–PEI combination, might provide a practical scaffold for sequestering metal ions in aqueous systems. In fact, PEI effectively stabilizes the TA–Fe ion chelated complex.[27] To substantiate this hypothesis, a column packed with PEI/TA-coated beads (3 mg, wet weight) was prepared to elute 5 mL of a 10 ppm Fe(III) ion solution down the column. The post-treatment concentration of Fe(III) was measured to be 3.65×10^{-7} moles. The noticeable shift to a reddish-purple color in the beads after iron-binding has visually confirmed the effective removal of iron from water.

TA is known to establish an octahedral coordination around iron ions.[26] To validate whether TA coordinates with iron ions *via* the chelation mechanism, Raman spectroscopy was performed on PEI/TA-coated beads before and after treatment with an Fe(III) solution. These beads were freeze-dried for two days prior to analysis. A Raman shift indicating TA's phenyl ring vibrations typically appear from ~1250 to ~1500 cm^{-1}. Concurrently, shifts associated with TA–Fe coordination generally appear between ~550 and ~650 cm^{-1}.[28,29] As demonstrated in Fig. 2c, the spectrum of PEI/TA (the black line) exhibited a single, broad peak at 1295.92 cm^{-1}, attributed to phenyl vibrations. This peak bifurcated into two narrower peaks at 1257.35 and 1348.66 cm^{-1} upon Fe(III) binding (the purple line). Also, the characteristic TA–Fe coordination peak emerged distinctly at 591.29 cm^{-1} exclusively for PEI/TA-Fe beads, highlighting the chelation of Fe ions by TA. The results showed that the Fe(III) removal mechanism is based on galloyl–Fe metal–phenolic coordination. Also, the Raman spectrum of the PEI/TA bead exhibited a sharp peak at 1593.2 cm^{-1}. This peak, when juxtaposed with the amine peak from pure PEI (~1689 cm^{-1}),[30] was shifted to slightly lower wave numbers, indicating the interactions with the phenolic hydroxyl groups of TA. Notably, the intensity of this peak was significantly decreased upon introducing iron ions to the PEI/TA beads, demonstrating the close interactions among the amine–iron ion–galloyl groups. This finding further provides an explanation (that will be explained later in Fig. 3d and 4, top and bottom photos) for the more pronounced color change observed in PEI/TA-coated beads compared to solely TA-coated beads when iron ions are present.

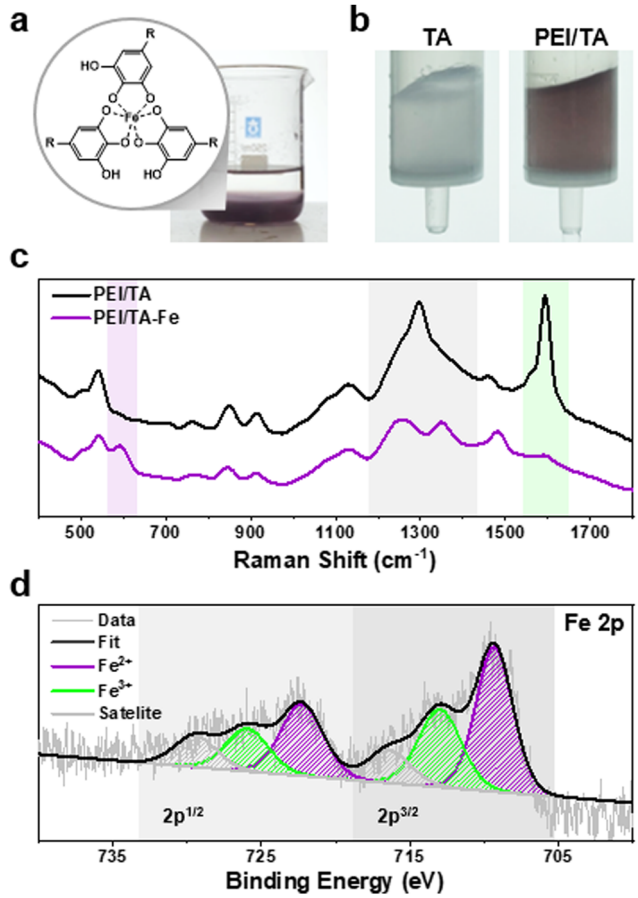

Fig. 2 Characterization of metal adsorption abilities of the PEI/TA-coated beads. (a) Schematic representation of galloyl–metal coordination chemistry. (b) Color change of the TA-coated beads (left) and PEI/TA-coated beads (right). (c) Raman spectrum of the PEI/TA-coated beads (black line) and Fe(III) eluted PEI/TA beads (purple line). (d) XPS analysis of the PEI/TA-coated beads after an iron solution was applied. Fe2p spectra for Fe(II) (purple) and Fe(III) (green).

The role of TA as a reducing agent has been well-documented.[31] Given the antioxidant properties of TA, we hypothesized that a considerable amount of the Fe ions would be reduced from Fe(III) to Fe(II) during the elution process. To verify this, we analyzed the iron (Fe2p) scan of the identical XPS samples. If our hypothesis is correct, peaks corresponding to Fe(II) and Fe(III) would be observed with a binding energy shift of about 3–4 eV for Fe2p photoelectrons, where Fe(II) $2p^{3/2}$: ~709–711 eV and Fe(III) $2p^{3/2}$: ~711–714 eV.[32,33] As shown in Fig. 2d (right), the Fe(II) $2p^{3/2}$ peak was detected at 709.3 eV (purple), and the Fe(III) $2p^{3/2}$ peak was detected 713.0 eV (green). Similarly, Fe(II) and Fe(III) photoelectron peaks for $Fe2p^{1/2}$ co-existed at 722.3 eV and 725.9 eV with a binding energy difference of 3.6 eV. These results confirm that the bound Fe(III) ions were reduced by redox coupling of TA upon coordination.

With the confirmation of successful iron adsorption capabilities, the sensitivity of removal–detection coupling was evaluated in real-time by the development of a deep-blue color upon Fe(III) coordination to TA/PEI. The precipitation model eliminates spatial constraints, facilitating more extensive contact between the beads and metal ions. First, 25 g of wet PEI/TA beads was dispersed in double-distilled water (DDW), stirring the bead solution at 300 rpm. As shown in Fig. 3a and b, binding of iron ions (equivalent to metal removal from water) simultaneously developed a deep purple color within a minute (5 ppm). Rapid color development was observed in just 20 seconds for a 5 ppm solution (Fig. 3a). The removal–detection coupling was able to monitor the capturing reaction for a sub-ppm concentration, 0.5 ppm. Because of the low concentration, the color development took a longer time of 40 seconds for

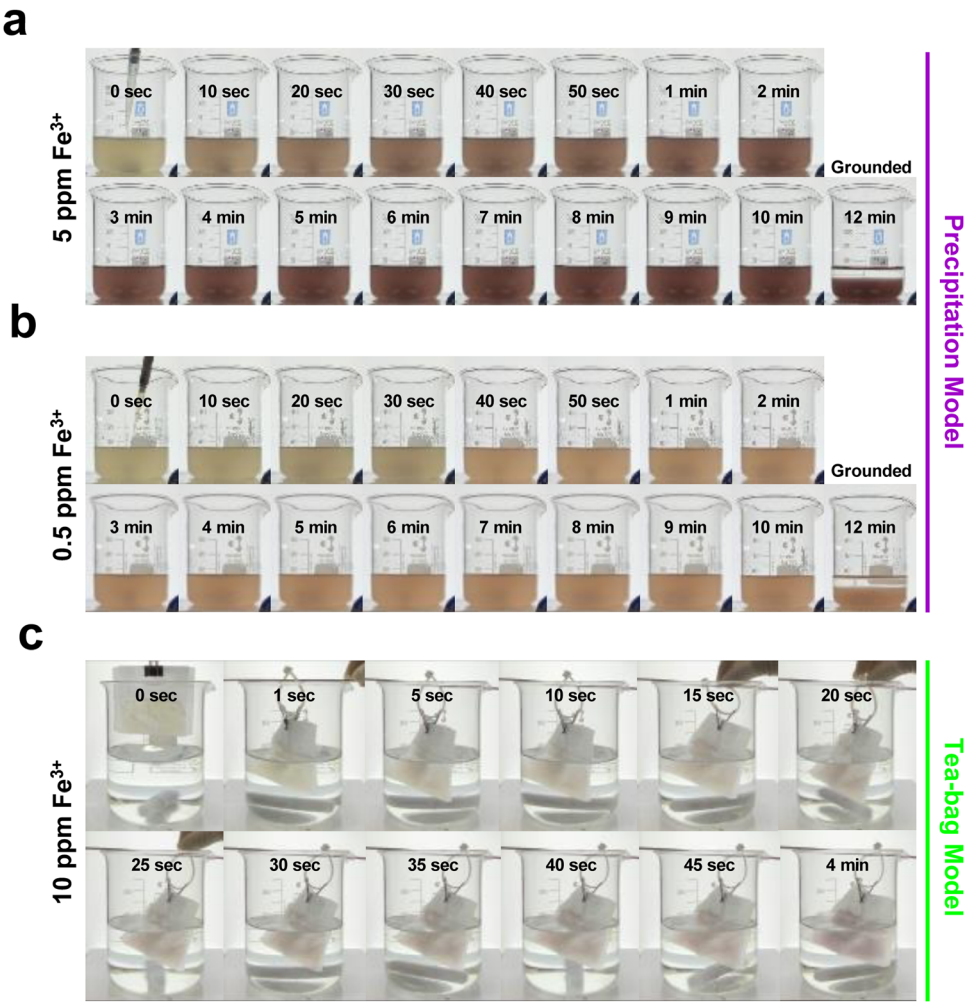

Fig. 3 Real-time monitoring of removal–detection coupling of iron ions as a function of time. Photographs of iron removal in (a) 5 ppm and (b) 0.5 ppm iron ion solutions. (c) Photographs of the tea-bag model for iron removal, where the PEI/TA-coated beads are contained in a tea-bag.

visual detection (Fig. 3b). Compared to existing ppm-level colorimetric detection methods,[34,35] the PEI/TA beads have achieved superior detection sensitivity down to the ppb-level. When operated under the 'tea-bag' configuration, there was a marginal reduction in the metal removal capacity to approximately $\sim$0.38 mg g^{-1}. This decrease might be attributed to spatial limitations experienced by the beads, in contrast to the unconstrained environment of the precipitation method.

While numerous existing chemical adsorption methodologies predominantly focus on the mere removal of metal ions, our polyphenol-amine chemistry offers a compelling difference. Specifically, it allows real-time visualization of metal removal as illustrated in Fig. 3c. The system's efficacy and sensitivity notably exceeded our initial expectations.

During the exposure of the tea-bag to a 10 ppm of Fe(III) solution, the beads underwent a discernible shift to a light pink hue in only 20 seconds. This hue intensified to deeper pink within 4 minutes, as evidenced by the last photograph in Fig. 3c. The inherent sensitivity of our polyphenol–gallol chemistry is underscored by its capacity to monitor metal–ion removal even from water with mere 0.5 ppm Fe(III) (Fig. 3b). In a comparative assessment, TA-only-coated beads (Fig. 4, top) displayed nearly no color change. In contrast, the PEI/TA-coated beads manifested a distinct purple color (Fig. 4, bottom), enabling the visual detection of iron ions.

Based on the results presented so far, the intricate chemical interplay among polyphenol, metal, and PEI can be elucidated as outlined in Fig. 4. Initially, the galloyl group's reductive capability results in the coexistence of both oxidation states of iron ions (II/III) (i). The electronic state is corroborated by XPS results (Fig. 2d). Subsequently, the oxidized galloyl–quinone (ii_a) undergoes a chemical reaction with the amines in PEI (ii_b). This leads to the formation of dual-ligand-associated coordination (–N–Fe–galloyl–) bonds (iii), forming a 1 : 1 : 1 (PEI : Fe(II/III) : TA) ternary complex. Additionally, there exists coordination solely mediated by TA's galloyl ligands (iv), forming a binary complex with a maximum ratio of 1 : 3 (Fe(II/III): TA). The interplay between amine and polyphenol intensifies the resulting coloration. As depicted in the provided photographs, a vivid deep purple color emerges upon the reaction involving PEI–gallol (lower). In contrast, a lighter purple shade was observed when only TA coated the bead surfaces (upper). This distinction

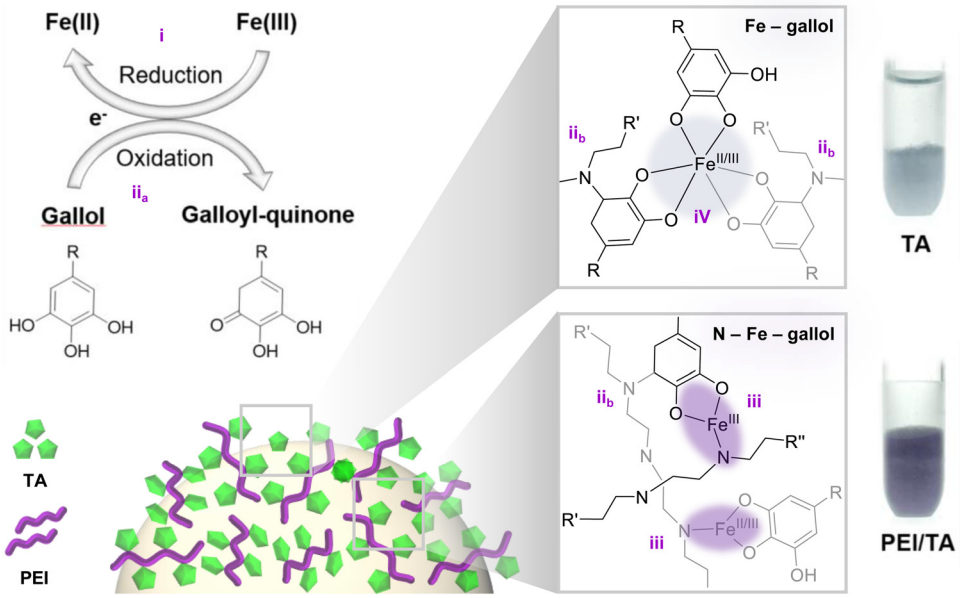

Fig. 4 The 'Detec-Ture' mechanism explaining how to couple metal removal and visual detection through the interplay of polyphenol–metal–amine.

clarifies why the PEI/TA-coated beads exhibited enhanced detection sensitivity down to a 1 ppm Fe solution. The feature was not observed in TA-coated beads (Fig. 3d).

Determining the iron removal capacity of PEI/TA-coated beads is crucial. For this purpose, an approach involving an excessive exposure of metal ions to the beads was considered appropriate. Thus, we adopted a precipitation method, wherein an excess of iron (10 ppm, 300 mL) was introduced to the beads. The iron solution was collected at 10-second intervals for the first 2 minutes, then every minute from 2–10 minutes, and finally every 10 minutes from 10–30 minutes. Subsequent ICP analysis of these solutions revealed that the iron binding capacity of the PEI/TA-beads was approximately 0.55 mg g^{-1}. When juxtaposed with prior research Fe adsorbents – specifically, alginate ($\sim$0.38 mg g^{-1}, pH = 4)[36] and wollastonite ($\sim$0.05 mg g^{-1}, pH = 4),[37] – the PEI/TA beads demonstrated commendable iron removal. Also, the binding of Fe(III) onto the PEI/TA beads follows a pseudo-second order kinetic model rather than a pseudo-first order model. The equation for pseudo-second order kinetics[38] is:

$$\frac{t}{q_t} = \frac{1}{k_2 q_e^2} + \frac{t}{q_e} \quad (1)$$

where k_2 (g mg^{-1} min^{-1}) represents the rate of pseudo-second order kinetics, q_t (mg g^{-1}) represents the Fe ion adsorption at a given time, and q_e (mg g^{-1}) represents the Fe ion adsorption at equilibrium (*i.e.*, saturated adsorption).

Utilizing the experimental outcomes shown in Table S1 (ESI†), a dot plot (time *vs.* t/q_t) can be drawn (Fig. 4a, red). When performing linear regression, a nearly perfect fit with an R^2 value of 0.999 was observed. In contrast, the pseudo-first order kinetics model did not provide a well-fitting result. The corresponding model equation is:

$$\ln(q_e - q_t) = \ln q_e - k_1 t \quad (2)$$

where k_1 (g mg^{-1} min^{-1}) represents the rate of pseudo-first order kinetics. Using the experimental results listed in Table S2 (ESI†), a dot plot (time *vs.* $\ln(q_e - q_t)$) was drawn (Fig. 4a, black). Linear regression results did not fit well with a low R^2 value of 0.82.

To further understand the adsorption mechanism of PEI/TA-coated beads toward Fe ions, two representative adsorption isotherm models were considered. The Langmuir isotherm model depicts Fe ion adsorption in a monolayer with uniform binding energy on a homogeneous surface, while the Freundlich isotherm suggests multi-layer adsorption on a heterogeneous surface.[37,39] The linear equations for Langmuir and Freundlich isotherm models are presented in eqn (3) and (4), respectively.

$$\frac{C_e}{q_e} = \frac{1}{K_L q_m} + \frac{C_e}{q_m} \quad (3)$$

$$\ln q_e = \ln K_f - n \ln C_e \quad (4)$$

Here, q_m designates the maximum adsorption capacity, K_L is the energy-related Langmuir constant, whereas K_F and $1/n$ stand for the Freundlich constants pertaining to capacity and Fe ion adsorption intensity, respectively. Fig. 5b demonstrates both the Langmuir (black, left and bottom axis) and Freundlich models (red, right and top axis), with parameters listed in Tables S3 and S4 (ESI†). The Freundlich model's R^2 value surpassed 0.999, notably exceeding that of the Langmuir model. Consequently, PEI/TA bead adsorption predominantly follows the Freundlich model, pointing to multi-layer adsorption on a heterogeneous surface. The confirmation of the Freundlich isotherm model in the iron ion adsorption system further supports the presence of a heterogenous surface involving amine and gallol, leading to color enhancement *via* –N–Fe–galloyl– interactions (Fig. 4iii) of the PEI/TA bead.

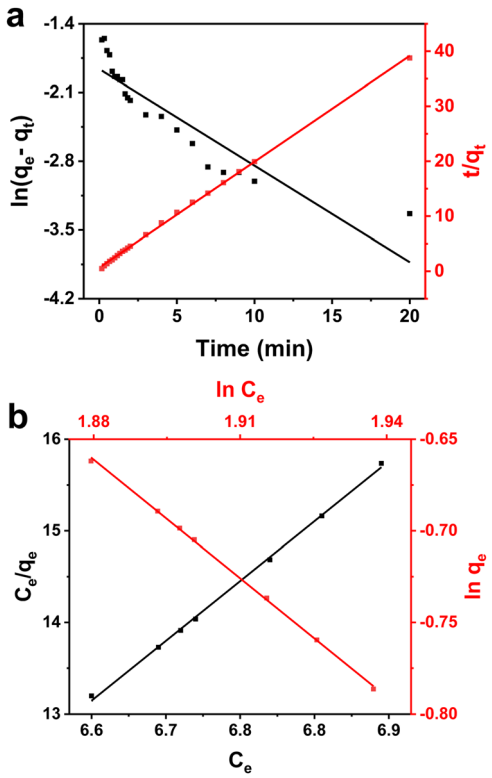

Fig. 5 Fe–ion adsorption mechanics of PEI/TA-coated beads. Plots of (a) the pseudo-first order model (black, left axis) and the pseudo-second order model (red, right axis) for the adsorption kinetics in the Fe ion solution. Plots of (b) the Langmuir isotherm model (black, left and bottom axis) and the Freundlich isotherm model (red, right and top axis) for the adsorption isotherm in the Fe ion solution.

Conclusions

In the evolving landscape of polyphenol–amine and polyphenol–metal surface chemistries, our work stands out by integrating polyphenols, amines, and metals for concurrent detection and capture of iron ions. The 'Detec-Ture' mechanism we introduce exhibits both real-time monitoring and sequestration, filling a noted gap in existing research. This approach efficiently addresses the challenges posed by abundant iron in water without relying on energy-intensive or complex methods. Impressively, PEI/TA-coated beads rapidly detected iron ions, with a sensitivity reaching 0.5 ppm, and displayed robust adsorption capabilities. Our findings not only showcase the potential of polyphenol–amine–metal networks but also illuminate a promising path for future endeavors in water purification and iron overload disease mitigation.

Author contributions

H. J. investigation, methodology, visualization, writing – original draft, and writing – review and editing; H. K. P. investigation, methodology, and visualization; J. W. methodology, visualization, and software; Y. R. N. software; E. K. methodology and visualization; J. S. methodology and visualization; H. L. conceptualization, funding acquisition, methodology, project administration, supervision, writing – original draft, and writing – review and editing.

Conflicts of interest

There are no conflicts to declare.

Acknowledgements

This research was supported by the National Research Foundation of Korea (NRF) grants funded by the Government of Korea (MSIT): Center for Multiscale Chiral Architectures, Science Research Center (SRC) Program (2018R1A5A1025208) and the Food and Drug Administration of South Korea (21173MFDS562).

References

1 H. Lee, S. M. Dellatore, W. M. Miller and P. B. Messersmith, *Science*, 2007, **318**, 426–430.
2 T. S. Sileika, D. G. Barrett, R. Zhang, K. H. Lau and P. B. Messersmith, *Angew. Chem., Int. Ed.*, 2013, **52**, 10766–10770.
3 H. Lee, J. Rho and P. B. Messersmith, *Adv. Mater.*, 2009, **21**, 431–434.
4 K. Lee, E. Prajatelistia, D. S. Hwang and H. Lee, *Chem. Mater.*, 2015, **27**, 6478–6481.
5 R. Xu, X. Huang, T. L. Hopkins and K. J. Kramer, *Insect Biochem. Mol. Biol.*, 1997, **27**, 101–108.
6 K. J. Kramer, M. R. Kanost, T. L. Hopkins, H. Jiang, Y. C. Zhu, R. Xu, J. L. Kerwind and F. Turecek, *Tetrahedron*, 2001, **57**, 385–392.
7 S. Hong, J. Yeom, I. T. Song, S. M. Kang, H. Lee and H. Lee, *Adv. Mater. Interfaces*, 2014, **1**, 1400113.
8 S. Hong, C. F. Schaber, K. Dening, E. Appel, S. N. Gorb and H. Lee, *Adv. Mater.*, 2014, **26**, 7581–7587.
9 H. K. Park, D. Lee, H. Lee and S. Hong, *Mater. Horiz.*, 2020, **7**, 1387–1396.
10 H. Ejima, J. J. Richardson, K. Liang, J. P. Best, M. P. V. Koeverden, G. K. Such, J. Cui and F. Caruso, *Science*, 2013, **341**, 154–157.
11 K. N. Raymond, E. A. Dertz and S. S. Kim, *Proc. Natl. Acad. Sci. U. S. A.*, 2003, **100**, 3584–3588.
12 G. P. Maier, M. V. Rapp, J. H. Waite, J. N. Israelachvili and A. Butler, *Science*, 2015, **349**, 628–632.
13 C. C. Hsu, N. H. Senussi, K. Y. Fertrin and K. V. Kowdley, *Hepatol. Commun.*, 2022, **6**, 1842–1854.
14 I. Radovenchyk, O. Ivanenko, M. K. Victorivna and V. Radovenchyk, *Ecol. Eng. Environ. Technol.*, 2023, **24**, 163–172.
15 M. D. Víctor-Ortega, J. M. Ochando-Pulido and A. Martínez-Ferez, *J. Ind. Eng. Chem.*, 2016, **36**, 298–305.
16 M. Shin, J. H. Choi, K. Kim, S. Kim and H. Lee, *ACS Appl. Mater. Interfaces*, 2021, **13**, 10741–10747.
17 J. Lee, E. Park, A. Fujisawa and H. Lee, *ACS Appl. Mater. Interfaces*, 2021, **13**, 21703–21713.
18 Y. Zhao, L. Xu, F. Kong and L. Yu, *Chem. Eng. J.*, 2021, **416**, 129090.

19 S. Y. Lee, Y. J. Jeong and W. H. Park, *Chemosphere*, 2022, **307**, 135719.
20 S. Jiang, S. Li, P. Zhang, H. Miao, P. Jiang and Y. Leng, *J. Environ. Chem. Eng.*, 2022, **10**, 108670.
21 K. W. Huang, C. J. Yu and W. L. Tseng, *Biosens. Bioelectron.*, 2010, **25**, 984–989.
22 A. Üçer, A. Uyanik and Ş. F. Aygün, *Sep. Purif. Technol.*, 2006, **47**, 113–118.
23 W. Wei, J. Li, X. Han, Y. Yao, W. Zhao, R. Han, S. Li, Y. Zhang and C. Zheng, *Sci. Total Environ.*, 2021, **778**, 146189.
24 A. E. Fazary, M. Taha and Y. H. Ju, *J. Chem. Eng. Data*, 2009, **54**, 35–42.
25 S. Berto and E. Alladio, *Front. Chem.*, 2020, **8**, 614171.
26 T. K. Ross and R. A. Francis, *Corros. Sci.*, 1978, **18**, 351–361.
27 Y. Wang, Y. Zhang, C. Hou, F. He and M. Liu, *New J. Chem.*, 2016, **40**, 781–788.
28 Q. Li, D. G. Barrett, P. B. Messersmith and N. Holten-Andersen, *ACS Nano*, 2016, **10**, 1317–1324.
29 A. Espina, M. V. Canamares, Z. Jurasekova and S. Sanchez-Cortes, *ACS Omega*, 2022, **7**, 27937–27949.
30 C. Chen, F. Chen, L. Liu, J. Zhao and F. Wang, *Electrochim. Acta*, 2019, **326**, 134964.
31 S. M. Burkinshaw and N. Kumar, *Dyes Pigm.*, 2009, **80**, 53–60.
32 M. A. Rahim, H. Ejima, K. L. Cho, K. Kempe, M. Müllner, J. P. Best and F. Caruso, *Chem. Mater.*, 2014, **26**, 1645–1653.
33 C. M. Maerten, L. Lopez, P. Lupattelli, G. Rydzek, S. Pronkin, P. Schaaf, L. Jierry and F. Boulmedais, *Chem. Mater.*, 2017, **29**, 9668–9679.
34 A. Choodum, W. Sriprom and W. Wongniramaikul, *Spectrochim. Acta, Part A*, 2019, **208**, 40–47.
35 M. F. Filgueiras and E. M. Borges, *J. Chem. Educ.*, 2022, **99**, 2067–2078.
36 A. Asthana, R. Verma, A. K. Singh, M. A. B. H. Susan and R. Adhikari, *Macromol. Symp.*, 2016, **366**, 42–51.
37 A. K. Singh, D. P. Singh, K. K. Pandayb and V. N. Singh, *J. Chem. Tech. Biotechnol.*, 1988, **42**, 39–49.
38 Y. S. Ho and G. McKay, *Process Biochem.*, 1999, **34**, 451–465.
39 O. P. Murphy, M. Vashishtha, P. Palanisamy and K. V. Kumar, *ACS Omega*, 2023, **8**, 17407–17430.